CONSEIL INTERNATIONAL
DES MACHINES A COMBUSTION

INTERNATIONAL COUNCIL
ON COMBUSTION ENGINES

PAPER NO.: 50

Optimization of Mixture Formation in Medium Speed Dual-Fuel and Gas Engines with Support of Advanced Optimization Techniques and Optical Measurements

Ulf Waldenmaier, MAN Diesel + Turbo SE, Germany
Stefan Djuranec, MAN Diesel + Turbo SE, Augsburg
Gunnar Stiesch, MAN Diesel + Turbo SE, Germany
Fridolin Unfug, KIT, Germany
Uwe Wagner, KIT, Germany

Abstract: For future gas and dual-fuel engines mixture formation is one of the most important development areas to fulfill upcoming emission legislations and to improve combustion efficiency. Therefore MAN Diesel & Turbo SE is optimizing the mixture formation of gas and dual-fuel engines with support of advanced CFD-optimization techniques and single cylinder engine measurements. Today's CFD-optimization of an intake port with gas admission pipe is an iterative process starting with an educated first guess design which has to be evaluated with simulation results and engine measurements. This evaluation is base of the first optimization loop. The experience of the CFD-engineer is the optimization tool in that process. In general 4 to 5 iterations are necessary to improve the mixture formation and flow behavior in the intake port. With this state of the art method it takes about two weeks to reach the design target for mixture formation. With advanced CFD-simulation and optimization tools it is possible to get the best possible design under consideration of the available design parameters within days. Nevertheless, the quality of the CFD-optimization is directly linked to the quality of CFD-simulation methods. The easiest way to validate mixture formation simulation results is an indirect validation with engine measurements. The validation is a comparison of the simulated mixture formation quality at start of ignition with engine measurements considering emissions, knocking behavior and gas consumption. For bigger variations this validation shows surprisingly good agreement. Still investigating flow details and a direct validation of the mixture formation is not possible. Up to now no optical investigations considering mixture formation in the intake port for large engines are known. To close this gap MAN Diesel & Turbo SE in cooperation with the Institut fuer Kolbenmaschinen of the Karlsruhe Institute of Technology have done PIV and Mie-scattering measurements on a modified flow bench for gas and dual-fuel engines. The measurements aimed on flow behavior and mixture formation for different gas admission pipes and intake valve seat rings for varying the flow behavior in the combustion chamber. The optical measurements helped to rise the quality of CFD-simulation methods and to improve the mixture formation of gas and dual-fuel engines to fulfill future emission legislation limits.

INTRODUCTION

One of the most important development fields within the gas combustion process for gas and dual-fuel engines is the flow behavior and mixture formation in the combustion chamber. Intake port and gas mixing device design directly influence charge motion, mixture formation, turbulence and so combustion and emission formation.

Mixture formation of gas and charge air starts in the intake port with the gas mixing device design. It is important to support the following mixing process in the combustion chamber with a good gas distribution during the intake phase of the gas exchange. Finally mixture formation and turbulence level as well are mainly influenced by the charge motion and combustion chamber design.

To find the best possible air-gas mixing and combustion chamber design modern CFD (CFD - Computational Fluid Dynamics) optimization techniques are an appropriate tool to support the development process for medium speed gas and dual-fuel engines to fulfill today's and future emission standards and to improve engine reliability and efficiency. However to ensure high quality results in the CFD-supported development process the CFD methods have to be of high quality as well. This can only be ensured by validation with engine tests and optical measurements on special test rigs respectively.

First indirect validations concerning turbulence level and gas mixing with SCE-tests (Single Cylinder Engine) showed surprisingly good agreement. To validate the CFD models in detail optical investigations for charge motion and mixture formation were performed on a blower test rig at the Institut für Kolbenmaschinen of the Karlsruhe Institute of Technology.

The following paper describes the CFD methods for simulating charge motion and mixture formation. The two methods will be discussed and also validated separately. Optical PIV-investigations (PIV - Particle Image Velocimetry) on a blower test rig for measuring charge motion for different intake port variations will be explained. Mie scattering measurements investigating the mixing process in the intake port were still in progress while writing this paper. Hence, Mie scattering measurements will be explained but will not be used for validation. The validation of the mixing performance will be done indirectly by comparing CFD-simulation results with SCE measurements under consideration of charge motion validation results from optical blower tests.

CFD-SIMULATION METHOD

Simulating charge motion and mixture formation was done by using steady-state CFD simulations with the commercial RANS (RANS - Reynolds averaged Navier-Stokes) software suite ANSYS CFX. Surface models of the interesting designs were prepared for meshing with an unstructured mesh topology. The geometry of interest included ports with valves and seat rings, charge air manifold, a gas mixer dummy as well as a liner dummy.

The inlet and exhaust faces of the simulation model were extruded by the length of one diameter and four diameters respectively in order to obtain stable simulation conditions. The tetrahedral meshing was done with the tool ICEM CFD, where an unstructured Delauney-based mesh was created. During the validation phase, several meshing strategies were tested. While the maximum tetrahedra edge size was kept the same at about 12mm for all meshes, refinements were applied in bulk volume and valve seat faces, so the minimum edge size reached 1.5mm (Figure 1). For simulations with a k-ε turbulence model, two prism boundary layers were added in combination with wall function usage where the y^+-value was adjusted to be larger than 30. A comparison with SST (Shear Stress Transport) turbulence model and wall layer resolution was performed as well. Herefore, 12 prism boundary layers with smooth transition were used to obtain a $y^+ < 3$.

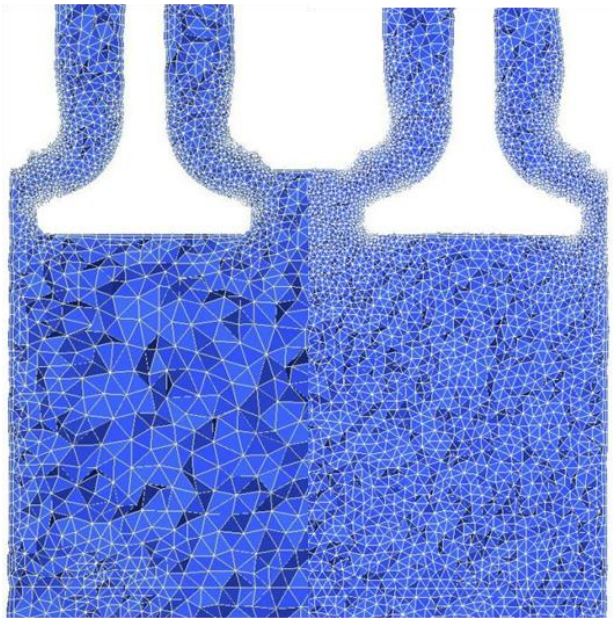

Figure 1: Cut through both valves along port and liner, with two boundary layers. Left half: coarsest mesh; Right half: finest mesh.

From inlet to outlet a constant pressure difference or, where available, air mass flow from measurements was imposed. The simulation domain was handled as compressible due to high velocities and pressure differences in some cases. As stated before, a k-ε turbulence model was used mostly, the SST model was taken only for comparison in some cases. The discretisation scheme was a blend of UW (UW – up wind) and CD (CD - central differences) with a dynamic blend factor [1].

As a result, the swirl number s_n was evaluated, which relates the flow axial rotation speed n_{rot} to the engine speed n_{Eng} for each valve lift and was calculated using the air density ρ, the engine displacement volume V_D and the air mass flow $\dot{m}_{Air}$ [2]:

$$s_n = \frac{n_{rot}}{n_{Eng}} = \frac{2\rho V_D n_{rot}}{\dot{m}_{Air}} \qquad \textit{Eq. 1}$$

The configuration was nearly the same for gas admission simulations. There, the real gas mixer geometry was included and a steady-state gas mass flow imposed at the appropriate boundary. The pressures and mass flows were adjusted to represent flow conditions at engine operation and maximum valve lift.

For these simulations, k-ε modeling was used with boundary layer as described above. Regions around the gas mixing device, especially around the exit holes, have been refined to reach a better resolution of the mixing zones. The fluid domain consisted of a two composition mixture of air and methane where a conservation equation was solved for the methane mass fraction. For that equation, the already mentioned blend of UW and CD discretisation was chosen.

The coefficient of variation $VarC$ of methane gas fraction at a plane near the valve seat face was chosen for mixing quality criteria. This is defined as the relation of standard deviation σ to the mean value $\bar{x}$ of methane fraction:

$$VarC = \frac{\sigma}{\bar{x}} \qquad \textit{Eq. 2}$$

OPTICAL INVESTIGATIONS ON BLOWER TEST BENCH

For investigating the influence of intake port design on flow behavior PIV investigations were performed by Schleh [3] for different intake port designs of MAN Diesel and Turbo SE dual-fuel engines on a blower test bench at Karlsruhe Institute of Technology. Figure 2 shows schematically the optical test set up which was applied.

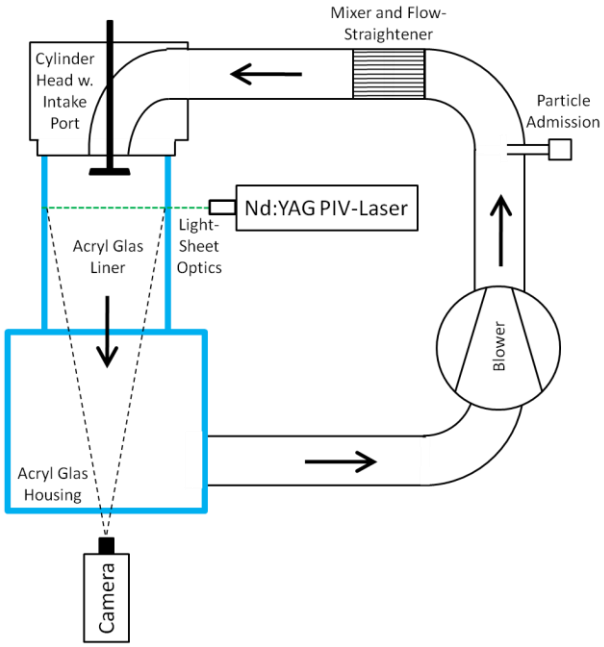

Figure 2: Optical test setup for PIV of flow behavior in the liner

The test bench was designed as a closed loop with a blower to generate a pressure difference of 10 mbar. Just after the blower the particle generator and mixing device was installed. After mixer and flow-straightener the mixture of air and particles was at an optimum before the flow entered the intake port. The intake valve lift was adjustable manually for different lifts.

For generating a laser sheet in the liner region an acryl glass liner was installed with the same inner diameter as the original liner. After the liner an acryl glass housing was necessary to guide the air-particle flow back to the compressor.

PIV investigations were done with a double shot camera and an Nd:YAG PIV-Laser. The principles of PIV-investigations are explained by Raffel et al [4] at length. The laser sheet was installed for different distances from the cylinder head to investigate the flow behavior along the liner axis. An exemplary view on the flow box flame deck is shown in Figure 3. Each PIV measurement consists of 200 particle images in order to get a good statistical information about the flow. The achieved PIV results will be discussed in the validation part of the CFD-simulations.

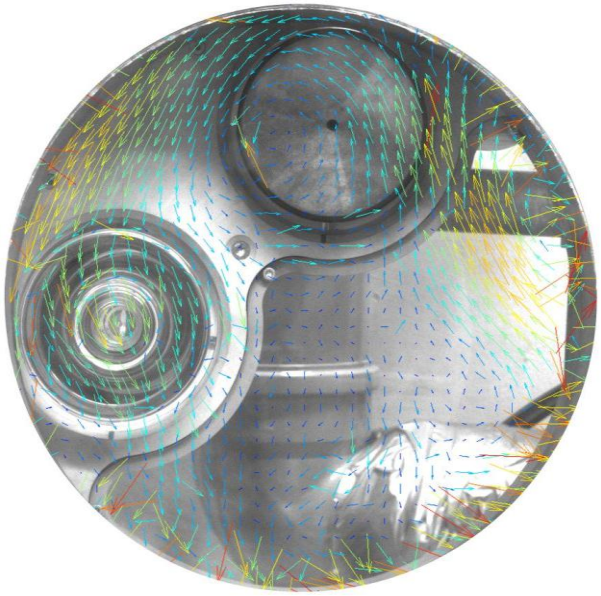

Figure 3: Raw PIV measurement with flow structure for maximum valve lift at 0.6 bore diameter distance from flame deck

The test set up for the Mie scattering technique measurements are much more complicated. In Figure 4 the test setup is explained schematically.

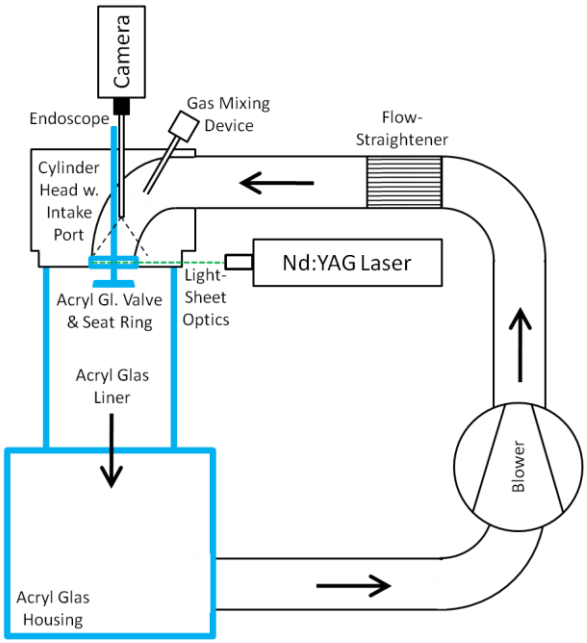

Figure 4: Optical test setup for scattering technique in the intake port

Also for the optical investigations in the intake port a closed loop test rig was used. Instead of particle admission before the flow straightener fog was introduced through the gas mixing device into the intake port. The Nd:YAG PIV-Laser sheet to illuminate the valve seat area was implemented through a polished acryl glass valve and an acryl glass valve seat ring. The distribution of fog in the valve seat area was observed with an endoscope mounted on a double shot camera. Figure 5 shows the view through the endoscope without fog admission for maximum valve lift.

Figure 5: Endoscopic view on intake valve seat area for maximum valve lift

As the optical investigations for mixture formation in the valve seat area were still in progress when writing this paper, the pre-validation of the CFD-simulation was done by comparing CFD-simulation results concerning mixture formation with SCE measurements.

COMPARISON OF CFD-SIMULATION AND OPTICAL INVESTIGATIONS

Evaluation of PIV measurements

The undertaken PIV measurements delivered information about the tangential velocity of the illuminated particles within the laser sheet (Figure 3). With this velocity information, a swirl number according to Eq. 1 was calculated. Herein, V_D followed from the engine geometry while the air mass flow $\dot{m}_{Air}$ was measured within the experiments. With the assumption that all PIV evaluation cells have the same size and no density differences occur, the axial rotation speed n_{rot} was calculated using the planar angular momentum of the flow:

$$n_{rot} = \frac{1}{2\pi}\omega = \frac{1}{2\pi}\frac{L}{I} = \frac{1}{2\pi}\frac{\sum_i m_i \vec{r}_i \times \vec{u}_i}{\sum_i m_i \vec{r}_i^{\,2}} \qquad \text{Eq. 3}$$

where ω is the angular velocity, L the angular momentum, I the moment of inertia, $\vec{r}_i$ the location vector of each cell, m_i its mass and $\vec{u}_i$ its velocity vector. Thus the swirl was calculated around the liner axis the coordinate system had to be adjusted such that its origin lies on this axis for a correct calculation of $\vec{r}_i$. The data underwent some post-processing where all velocity values were filtered to prevent unreasonably high runaway values. Also visible from Figure 3 is that near the liner wall, the velocity information became arbitrary and was not reliable. In order to circumvent this uncertainty and retain comparability with former paddle wheel swirl measurements, only values within a diameter of 0.7 liner bore were used for swirl calculations.

In Figure 6, measured velocity contours for sample geometry are depicted at a laser sheet positioned 0.65 bore diameter downstream of the flame deck. As shown in Figure 2 and Figure 3, the view is upstream towards the flame deck. For low valve lift, there is no bulk swirl motion visible but several counter-rotating flow structures may be identified. It was to expect that at this lift, the swirl number was near zero, and that the flow was very sensible to slight variations in geometry and environment conditions.

At middle valve lift, these flow structures mainly do not exist. The centered zone with higher velocity was weakened also. Instead, the flow became more structured, already first bulk swirling motion could be observed.

At maximum valve lift finally, there is one large-scale flow pattern developed. But this is not concentric with the liner axis. Instead, the vortex center is positioned quite close to the liner wall, resulting in high flow velocities at that half of the liner and low velocities at the other half. With respect to the PIV results presented it seems disputable whether the conventional swirl measurement technique with paddle wheels delivers enough sensible information for engine development and CFD validation.

In Figure 7, the evaluation of measured swirl value, normalized by the absolute value of swirl number at maximum valve lift, is shown for the three measured valve lifts. The swirl axis is defined to point liner-upwards thus negative swirl number means counter-clockwise rotation in Figure 6. The observations stated before are being confirmed by the evaluation. Very weak swirl, here with a slightly positive value, is obtained at low valve lift while at middle lift the negative flow direction is already visible. At high lift, the swirl reaches its highest value for this series of measurements

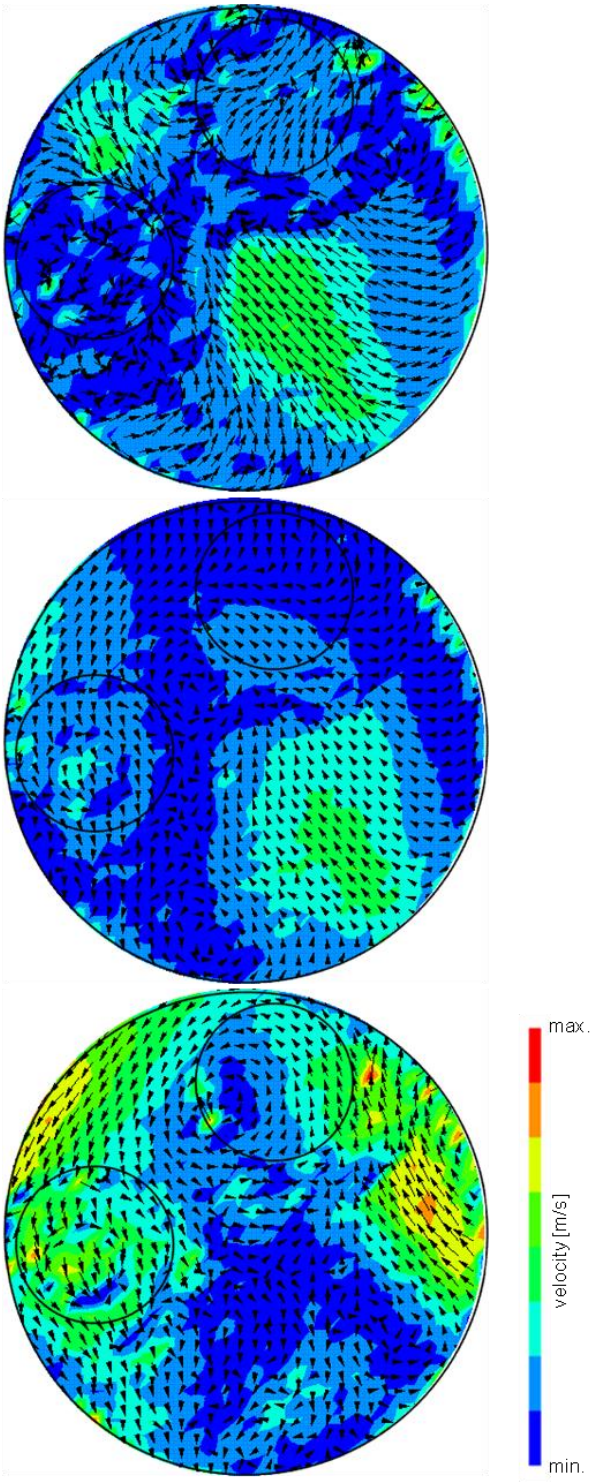

Figure 6: Velocity measured with PIV for sample geometry at 0.65 bore away from cylinder head at small (top), medium (middle) and maximum (bottom) valve lift.

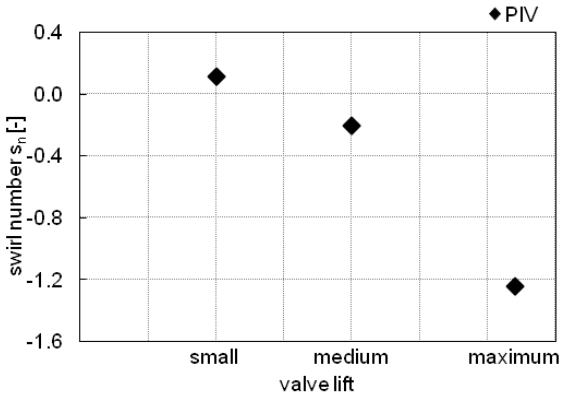

Figure 7: Normalized swirl number from PIV measurements for small, medium and maximum valve lift.

CFD Simulation Results with Base Turbulence Parameters

The same swirl evaluation methodology as depicted above for PIV measurements was applied for evaluation of the swirl number from CFD. Here, velocities for each cell were extracted at the position of the laser sheet from measurements. In this way, comparability of PIV and CFD data was guaranteed. In order to track the convergence and stability of the steady-state simulations, the swirl number evaluation was automated and executed after each iteration.

First simulations were performed with a coarse mesh at different valve lifts. There, convergence behavior was very weak and could not be improved by tuning of relaxation / damping factors in the simulations. Especially the swirl number showed unstable behavior such that it was not possible to create meaningful steady-state flow results.

The next step was to try more exact turbulence modeling to resolve separation and reattachment phenomena more accurately. So calculations with SST model and boundary layer resolving were done. Figure 8 shows a cut through a valve with velocity plotted after 500 iterations comparing k-ε and SST turbulence model. Both calculations have been done with similar, fine grid (as shown in Figure 1) while the mesh used for the SST model included twelve boundary layers, the mesh for k-ε was done with two layers. As can be seen in the figure, the k-ε model shows less pressure induced separation which is visible especially near the port bend and the valve seat rings. But the better boundary resolution still did not bring a gain in simulation stability or accuracy in swirl number calculation. So the conclusion was made that the cause for it was lying in the free flow after the valves as highlighted in Figure 8 where the SST model in fact acts like k-ε [5]. This was affirmed by a mesh study which did not bring any stability improvements. A detailed view into the simulation residuals showed that with a finer mesh only more vortex structures were resolved which resulted in new instabilities in simulation.

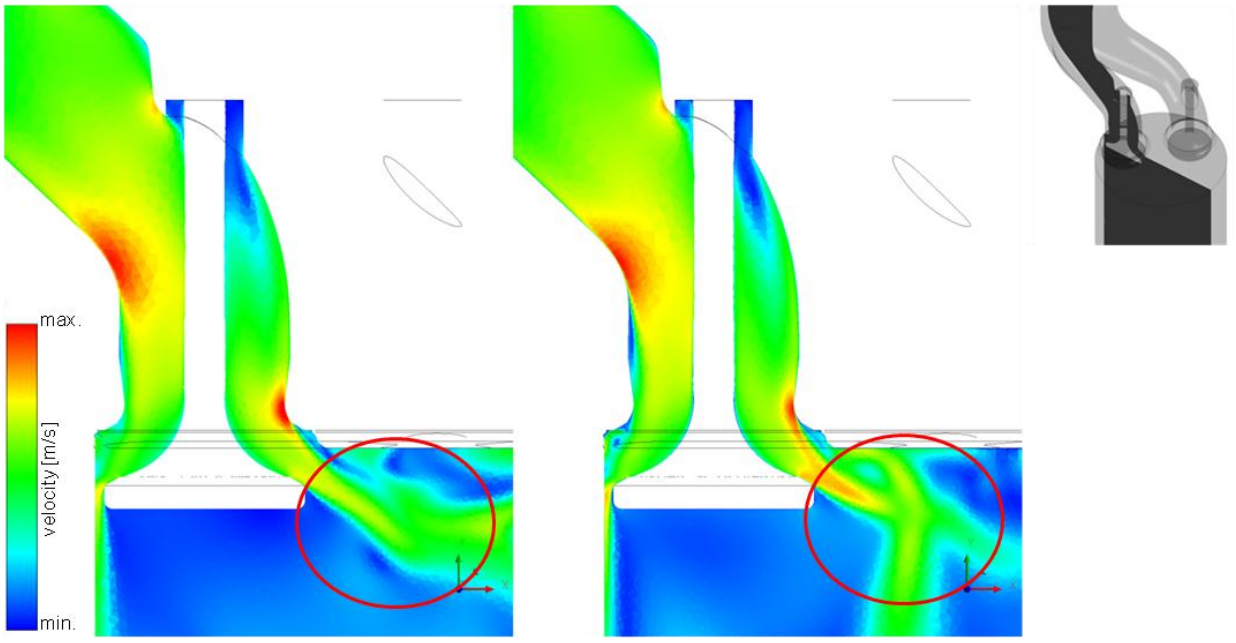

Figure 8: Velocity in valve region with k-ε and two boundary layers (left) versus SST and twelve boundary layers (right).

Turbulence Parameter Variation and Effect on Simulation Results

The reason for the instabilities and thus high residuals was found in the high shear flows in the valve region where the separated valve jets on one hand penetrate into the bulk region and on the other hand the flows from both valves collide. From publications [6, 7] and inhouse experience [8] is known that the standard k-ε turbulence parameters do not fit for all flow situations. Thus the approach was followed to optimize these parameters and so take influence on the turbulent eddy viscosity.

For the parameter optimization, a DOE (DOE – Design Of Experiments) parameter variation was used. With each parameter set, simulations were performed for all three valve lifts. The swirl number and its stability were chosen to serve as quality criteria for the given parameter set. After this a response surface was created which gave information about the influence of each parameter onto the simulation results. As last step, several parameter configurations were elaborated and their quality was checked with new simulations.

With the best parameter set, the simulation stability could be improved drastically with same damping factors as used with standard turbulence parameters. The steady-state simulations then converged or moved into a stable oscillation which made averaging possible. Figure 9 depicts the simulated velocities in a plane according to the laser sheet in PIV flow box for the finest mesh. The simulation results show very good agreement with measurements. Especially at small and middle valve lift, the main eddy patterns could be resolved properly in orientation and length scale. The velocity scale is also in good agreement with measurement. At maximum valve lift, the simulation results seem to be worse. There the eddy orientation is slightly rotated and less asymmetric compared to PIV.

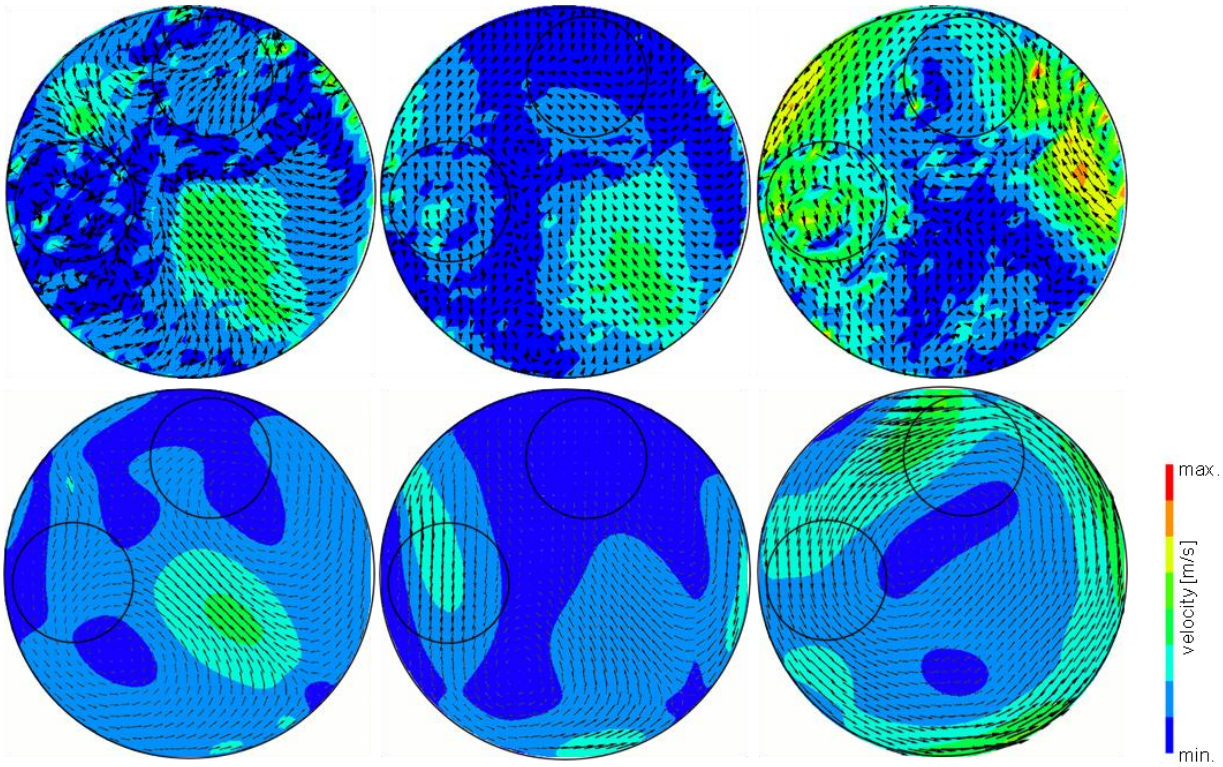

Figure 9: Comparison of velocities from PIV (top) and CFD (bottom) simulated with same turbulence parameter set from optimization, for low (top), medium (middle) and maximum (bottom) valve lift.

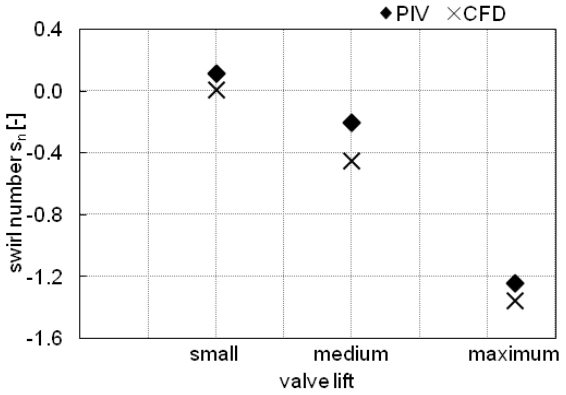

Figure 10: Comparison of stationary swirl number from PIV and CFD with best turbulence parameter set.

For these simulations, the swirl number was evaluated and compared with PIV measured values. Such a comparison is shown in Figure 10. The agreement of simulation with measurement is very good. The tendency in direction and scale is followed with good accuracy especially at large valve lift which is of most interest. The swirl values from simulation tend to be lower than measurement. This might be caused by the natural swirl creation of the given geometry which produces a negative swirl. The simulation seems to follow this natural swirl creation.

VALIDATION OF MIXTURE FORMATION ON SINGLE CYLINDER ENGINE

CFD Results for Gas Mixing

For validation of mixing device development, three device design variants were included in separate simulations using the methodology as depicted above. Starting from a base design, the devices have been created by varying several parameters like number and diameter of holes, device length, device orientation, and others (*Figure 11*).

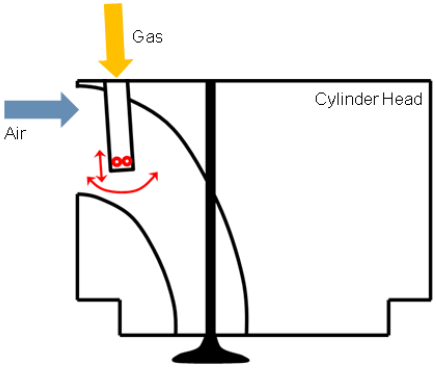

Figure 11: Base mixing device design proposal and location.

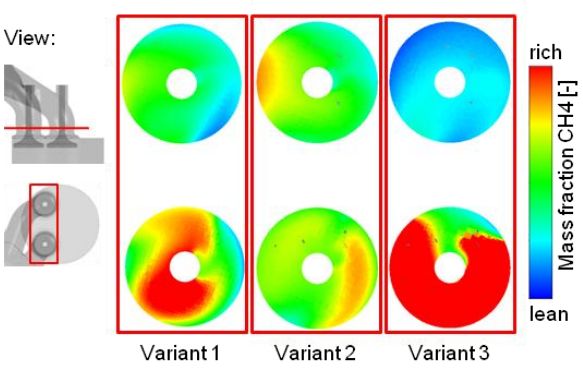

Figure 12: CFD simulation of gas mixing for three different gas mixing devices.

The most important criterion for estimation of design quality was the mixture homogeneity at a plane near the valve seat face shown in Figure 12.

As can be seen there, mixer design 2 showed the best overall mixture homogeneity. The distribution of gas onto both ports was also very good with this mixer. Vice versa, variant 3 performed worst. The methane was concentrated almost completely in the lower port arm and showed bad distribution. Variant 1 delivered results in between mixer 1 and 3 concerning gas homogeneity and distribution to both ports.

The observations made with Figure 12 were affirmed by the coefficient of variation ($VarC$) of methane fraction at the plane shown. As expected, variant 2 delivers the lowest and thus best $VarC$ value, while variant 3 shows the highest. Thus it was to expect that mixer 3 shows worst and mixer 2 best engine performance data as the mixture homogeneity influences strongly the exhaust emissions, knocking behavior and gas consumption of the engine. Because no optical measurements were available simulations were validated against single cylinder engine data.

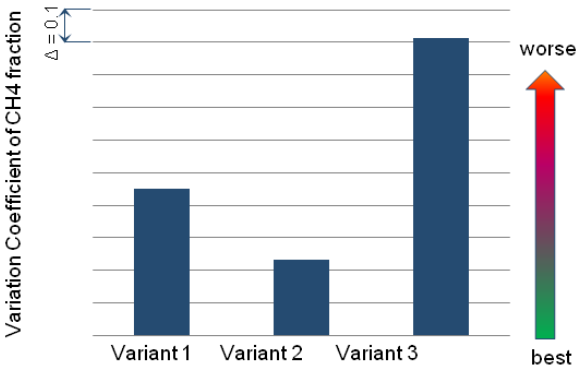

Figure 13: Variation Coefficient of CH4 fraction at plane from Figure 12.

Comparison with engine data

A good indicator for the mixing quality is the NO_x emission, but this is depending on in-cylinder gas temperatures, equivalence ratio, engine load and combustion duration. So for validation of the simulations, it was important to find similar conditions which allowed direct comparison of performance data with simulations. Nevertheless there is an incertitude by comparing indirectly CFD results with engine measurements.

These results are summarized in Figure 14. While at leaner air excess ratio λ the engine reacted less sensible to the mixer design, at rich λ values the difference was clear resulting in extraordinarily higher NO_x output with mixing device 3. Although simulations showed large differences in mixing between designs 1 and 2, the NO_x emission difference was within measurement tolerance so no trend was visible for these two designs.

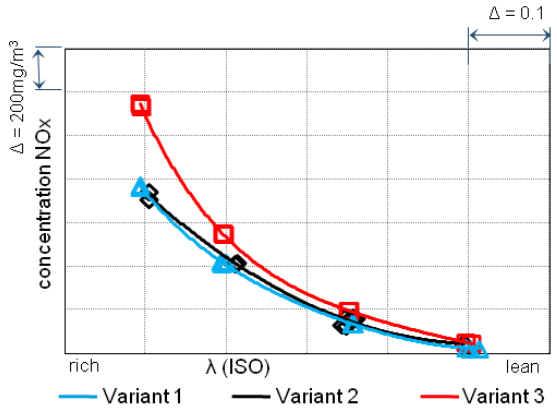

Figure 14: Engine performance results for the mixer variants in NO_x emissions over air excess ratio λ.

From this comparison it could be stated that the validation of gas mixing simulations with engine performance data was indirect and came with some difficulties. While the design with the best CFD results delivered a good overall performance, the trend from simulations was not being reproduced sufficiently within engine operation. So direct CFD validation with optical measurements cannot be substituted.

CONCLUSIONS

Today simulating charge motion and mixture formation is state of the art within the development process of medium speed gas and dual-fuel engines. However, commercial CFD simulation suites are developed and validated mainly for automotive applications. Due to the immense deviation between automotive and medium speed engine size it is not possible to keep same mesh sizes for both applications. So, big influence of meshing and applied turbulence models on simulation results can be expected for medium speed engines.

Charge motion validation with PIV measurements on a blower test bench showed that with standard turbulence model parameters it was not possible to get good agreement between simulated and measured swirl number and charge motion. With suitable meshing method and adjusted turbulence model parameters good agreement was achieved for different valve lifts.

Mixture formation was validated with SCE measurements for different mixing device designs. The indirect validation was done by comparing quality of simulated mixture formation in the intake valve seat region with measured engine out emissions for NO_X. With the improved charge motion simulation method the dependency of mixture formation quality and engine emissions was not reproduced sufficiently.

Further investigations concerning mixture formation will aim on direct validation of mixture formation in the intake valve seat region with mentioned Mie scattering measurements on the blower test bench. The improved simulation method for estimating charge motion and mixture formation has then to be verified for different intake port designs and swirl numbers. Additionally the influence of modified turbulence parameters on combustion simulation has to be investigated in detail.

NOMENCLATURE

CD	Central Differences discretisation	
CFD	Computational Fluid Dynamics	
DOE	Design Of Experiments	
PIV	Particel Image Velocimetry	
RANS	Reynolds Averaged Navier-Stokes	
SCE	Single Cylinder Engine	
SST	Shear Stress Transport	
UW	Up Wind discretisation	
I	Moment of inertia	kg m²
L	Angular momentum	kg m²/s
λ	Air excess ratio	
m_{Air}	Air mass flow	kg/s

m_i	Cell mass	kg
n_{Eng}	Engine speed	rps
n_{rot}	Axial rotation speed	rps
$\vec{r}_i$	Location vector of cell	m
ρ	Density	kg/m³
s_n	Swirl number	
$s_{n,max}$	Maximum swirl number	
σ	Standard deviation	
$\vec{u}_i$	Measured velocity of cell	m/s
$VarC$	Coefficient of variation	
V_D	Displacement volume	m³
ω	Angular velocity	1/s
$\bar{x}$	Mean value	
y^+	Dimensionless wall distance of first cell	

ACKNOWLEDGEMENTS

This work is part of the European Community integrated project “HERCULES-C – Higher Efficiency, Reduced Emissions, Increased Reliability and Lifetime, Engines for Ships”.

REFERENCES

[1] ANSYS Inc. “Discretisation of the governing equations - CFX Theory Guide”, ANSYS 13.0 Help, 2010

[2] THIEN, G. “Entwicklungsarbeiten an Ventilkanälen von Viertakt-Dieselmotoren“, Österreichische Ingenieur-Zeitschrift, Heft 9, Jg. 8, 1965

[3] SCHLEH H. "Experimentelle Untersuchung der Strömungsgeschwindigkeiten eines mittel-schnelllaufenden Dieselmotors mittels Particle Image Velocimetry", Diploma Thesis, Karlsruhe Institute of Technology, 2012

[4] RAFFEL M., WILLERT C., WERELEY S., KOMPENHANS J. “Particle Image Velocimetry - A Practical Guide”, Springer Verlag, 2007

[5] MENTER, F. R. Two-Equation Eddy-Viscosity Turbulence Models for Engineering Applications, AIAA Journal, Vol. 32, No. 8, pp. 1598-1605, 1994

[6] RODI, W. “Turbulence Models and Their Application in Hydraulics”, Progress in Energy and Combustion Science, Vol. 9, page 1-76, 1983

[7] POPE, S.B. “An Explanation of the Turbulent Round-Jet/Plane-Jet Anomaly”, AIAA Journal, Vol. 16 No. 3, page 279-281, 1978

[8] WALDENMAIER, U. “Berechnung der Verbrennung in schwerölbetriebenen Groß-dieselmotoren“, Südwestdeutscher Verlag für Hochschulschriften, 2009